Optical Engineering

OpticalEngineering.SPIEDigitalLibrary.org

Enhancement of light absorption efficiency of amorphous-silicon thin-film tandem solar cell due to multiple surface-plasmon-polariton waves in the near-infrared spectral regime[1*]

Muhammad Faryad
Akhlesh Lakhtakia

SPIE.

Enhancement of light absorption efficiency of amorphous-silicon thin-film tandem solar cell due to multiple surface-plasmon-polariton waves in the near-infrared spectral regime*

Muhammad Faryad
Akhlesh Lakhtakia
Pennsylvania State University
Department of Engineering Science and Mechanics
Nanoengineered Metamaterials Group (NanoMM)
University Park, Pennsylvania 16802-6812
E-mail: faryad@psu.edu

Abstract. The reflectances of a thin-film solar cell were computed, using the rigorous coupled-wave approach, as functions of the angle of incidence and the free-space wavelength for illumination by linearly polarized plane waves. A tandem solar cell made of amorphous-silicon alloys was considered. The metallic back-reflector was taken to be periodically corrugated. Both the simple and the compound periodic corrugations of the metallic back-reflector (surface-relief gratings) were investigated. Low-reflectance bands in the reflectance spectrums were correlated with the solutions of the underlying canonical boundary-value problem to delineate the excitation of multiple surface-plasmon-polariton (SPP) waves. For the standard AM1.5 solar irradiance spectrum, we found that the light absorption efficiency in the near-infrared spectral regime can be increased up to 100% when multiple SPP waves of both linear polarization states are excited. [DOI: 10.1117/1.OE.52.8.087106]

Subject terms: surface plasmon-polariton wave; grating coupling; compound grating; tandem solar cell.

Paper 130773P received May 29, 2013; revised manuscript received Jul. 4, 2013; accepted for publication Jul. 9, 2013; published online Aug. 16, 2013; corrected Dec. 3, 2014.

1 Introduction

Commercial silicon solar cells have a thickness of about 50 to 100 μm to absorb as much light as possible, especially in the near-infrared regime.[1] Excessive thickness of the solar cell does not only increase its manufacturing cost but also its carbon footprint during its manufacture. To reduce both, thin-film photovoltaic (PV) solar cells made of amorphous and polycrystalline silicon are being actively investigated.

The absorption efficiency of these thin-film solar cells can be improved by incorporating antireflection coatings[2–4] and texturing of the front surface.[5–7] The metallic back-reflector of a solar cell can also be textured at transverse length scales greatly larger than a thousand nanometers, but planar backing appears to perform better.[8] In contrast, periodic texturing of the metallic back-reflector was indicated even in the early 1980s to help absorb light better, if the period were a few hundred nanometers.[9] Hence, the use of a metallic surface-relief grating as the back-reflector may result in higher efficiency.[10,11]

A metal/semiconductor interface can guide surface-plasmon-polariton (SPP) waves. This was appreciated by Anderson in the 1980s,[12,13] but the prism-coupled technique suggested to exploit the broad solar spectrum seems not to have gained traction in the research community. A few years ago,[14] research interest returned when it was realized that an electric field of large magnitude, existing close to the back-reflector inside the semiconductor when an SPP wave is excited, is favorable to the generation of electron–hole pairs.

In single-junction amorphous-silicon (a-Si) solar cells backed by a periodically corrugated metallic back-reflector, the semiconductor is almost homogeneous. Therefore, only one SPP wave, that too of the p-polarization state, can be launched at a given free-space wavelength of light,[15,16] leading to modest gains in light absorption efficiency.[14,17] But multiple SPP waves of both linear polarization states can be guided by a periodically corrugated metal/semiconductor interface, if the semiconductor is periodically nonhomogeneous along the direction normal to the mean plane of the metal/semiconductor interface; this results in enhanced absorption of light of both linear polarization states, according to a predecessor study.[18] However, the semiconductor in that study[18] was taken to have a continuously varying relative permittivity, which is not easily implementable.

Therefore, we set out to theoretically investigate the usefulness of exciting multiple SPP waves in a realistic tandem solar cell with a piecewise homogeneous semiconductor, as shown schematically in Fig. 1. The solar cell is supposed to be made of a-Si alloys, and the metallic back-reflector is periodically corrugated. The a-Si alloys can be fabricated using plasma-enhanced chemical vapor deposition over planar and patterned substrates.[19] The composition of the alloys can be controlled by controlling the ratio of precursor gases (e.g., silane, hydrogen, methane, and germane) and the deposition temperature.[20] A top layer of aluminum-doped zinc oxide (AZO) allows electrical contact. Also, an AZO layer is sandwiched between the metal and the semiconductor to avoid the deterioration of the electrical properties of the a-Si alloy closest to the metal.[1]

*This paper is substantially based on the paper entitled "Efficiency enhancement of amorphous-silicon tandem solar cell due to multiple surface-plasmon-polariton waves," presented at the SPIE Conference 8620 Physics, Simulation, and Photonic Engineering of Photovoltaic Devices II, held February 2–7, 2013, in San Francisco, California.

0091-3286/2013/$25.00 © 2013 SPIE

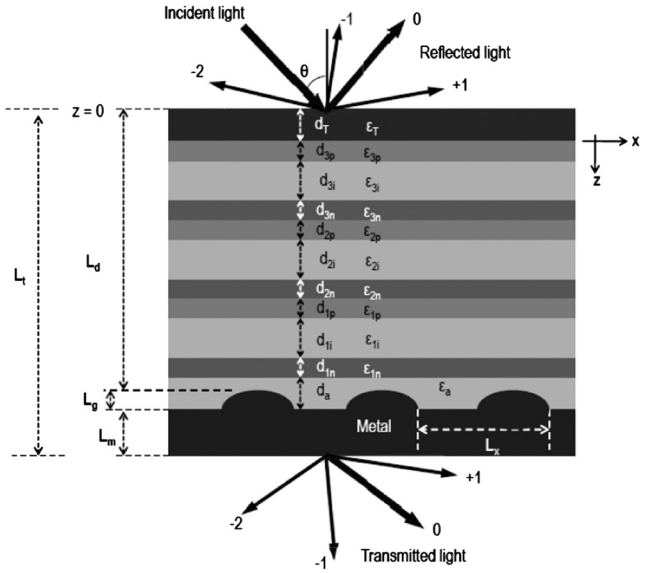

Fig. 1 Schematic of the tandem solar cell with a periodically corrugated metallic back-reflector. Specular components of the reflected and transmitted light are identified as of order 0, whereas nonspecular components are identified as of nonzero orders.

The plan of this paper is as follows. The methodology for computation is provided in brief in Sec. 2, and the numerical results are presented in Sec. 3. Concluding remarks are presented in Sec. 4. An $\exp(-i\omega t)$ dependence on time t is implicit, with ω denoting the angular frequency and $i = \sqrt{-1}$. The free-space wavenumber, the free-space wavelength, and the intrinsic impedance of free space are denoted by $k_0 = \omega\sqrt{\epsilon_0\mu_0}$, $\lambda_0 = 2\pi/k_0$, and $\eta_0 = \sqrt{\mu_0/\epsilon_0}$, respectively, with μ_0 being the permeability and ϵ_0 the permittivity of free space. Vectors are in boldface, and the Cartesian unit vectors are identified as $\hat{\mathbf{u}}_x$, $\hat{\mathbf{u}}_y$, and $\hat{\mathbf{u}}_z$.

2 Methodology

2.1 *Periodically Corrugated Metallic Back-Reflector*

Let us consider the boundary-value problem shown schematically in Fig. 1. The regions $z < 0$ and $z > L_t = L_d + L_g + L_m$ are vacuous, the region $0 < z < L_d$ is occupied by a dielectric material with a piecewise homogeneous relative permittivity $\epsilon_d(z)$ to be specified in Sec. 3, and the region $L_d + L_g < z < L_t$ by a metal with a spatially uniform relative permittivity ϵ_m. The region $L_d < z < L_d + L_g$ contains the periodically corrugated interface of period L_x along the x-axis. The relative permittivity $\epsilon_g(x,z) = \epsilon_g(x \pm L_x, z)$ in the reference unit cell of this region is given by

$$\epsilon_g(x,z) = \epsilon_d(z) + [\epsilon_m - \epsilon_d(z)]\mathcal{U}[z - g(x)], \quad x \in (0, L_x), \quad z \in (L_d, L_d + L_g). \tag{1}$$

Here, $g(x)$ is the grating-shape function, and

$$\mathcal{U}(\zeta) = \begin{cases} 1, & \zeta \geq 0 \\ 0, & \zeta < 0 \end{cases} \tag{2}$$

is the unit step function. All relative permittivities are frequency dependent.

To find the reflectance and transmittance of this solar cell when a linearly polarized plane wave is incident on it, the rigorous coupled-wave approach (RCWA)[21,22] was used. The adoption of this method for a piecewise homogeneous partnering dielectric material has been explained elsewhere,[16,23,24] and only a brief description is provided here.

In the vacuous half-space $z < 0$, let a plane wave, propagating in the xz plane at an angle θ with respect to the z-axis, be incident on the solar cell. Hence, the incident, reflected, and transmitted electric field phasors can be written in terms of Floquet harmonics as follows:

$$\mathbf{E}_{\rm inc}(\mathbf{r}) = \sum_{n\in\mathbb{Z}} (\mathbf{s}_n a_s^{(n)} + \mathbf{p}_n^+ a_p^{(n)}) \exp[i(k_x^{(n)} x + k_z^{(n)} z)], \quad z < 0, \tag{3}$$

$$\mathbf{E}_{\rm ref}(\mathbf{r}) = \sum_{n\in\mathbb{Z}} (\mathbf{s}_n r_s^{(n)} + \mathbf{p}_n^- r_p^{(n)}) \exp[i(k_x^{(n)} x - k_z^{(n)} z)], \quad z < 0, \tag{4}$$

$$\mathbf{E}_{\rm tr}(\mathbf{r}) = \sum_{n\in\mathbb{Z}} (\mathbf{s}_n t_s^{(n)} + \mathbf{p}_n^+ t_p^{(n)}) \exp\{i[k_x^{(n)} x + k_z^{(n)} (z - L_t)]\}, \quad z > L_t, \tag{5}$$

where $\mathbb{Z} \equiv \{0, \pm 1, \pm 2, \dots\}$,

$$k_x^{(n)} = k_0 \sin\theta + n q_x, \tag{6}$$

$$k_z^{(n)} = \begin{cases} +\sqrt{k_0^2 - (k_x^{(n)})^2}, & k_0^2 > (k_x^{(n)})^2 \\ +i\sqrt{(k_x^{(n)})^2 - k_0^2}, & k_0^2 < (k_x^{(n)})^2 \end{cases}, \tag{7}$$

and $q_x = 2\pi/L_x$. The unit vectors

$$\mathbf{s}_n = \hat{\mathbf{u}}_y \tag{8}$$

and

$$\mathbf{p}_n^{\pm} = \mp \frac{k_z^{(n)}}{k_0} \hat{\mathbf{u}}_x + \frac{k_x^{(n)}}{k_0} \hat{\mathbf{u}}_z \tag{9}$$

represent the s- and p-polarization states, respectively. The coefficients of the n'th-order Floquet harmonics in the incident, reflected, and transmitted electric field phasors are $a_{s,p}^{(n)}$, $r_{s,p}^{(n)}$, and $t_{s,p}^{(n)}$, respectively. The index $n = 0$ for specular components, whereas nonspecular components are indicated by $n \neq 0$.

In the RCWA, the relative permittivity in the region $0 < z < L_t$ is expanded as a Fourier series with respect to x, viz.,

$$\epsilon(x,z) = \sum_{n\in\mathbb{Z}} \epsilon^{(n)}(z) \exp(in\, q_x x), \quad z \in (0, L_t), \tag{10}$$

where $\epsilon^{(n)}(z)$ can be stated piecewise. The field phasors are written in the same region in terms of Floquet harmonics as

$$\left.\begin{aligned}\mathbf{E}(\mathbf{r}) &= \sum_{n\in\mathbb{Z}} [E_x^{(n)}(z)\hat{\mathbf{u}}_x + E_y^{(n)}(z)\hat{\mathbf{u}}_y + E_z^{(n)}(z)\hat{\mathbf{u}}_z]\exp(ik_x^{(n)}x) \\ \mathbf{H}(\mathbf{r}) &= \sum_{n\in\mathbb{Z}} [H_x^{(n)}(z)\hat{\mathbf{u}}_x + H_y^{(n)}(z)\hat{\mathbf{u}}_y + H_z^{(n)}(z)\hat{\mathbf{u}}_z]\exp(ik_x^{(n)}x)\end{aligned}\right\},$$
$$z\in(0,L_t), \tag{11}$$

with unknown scalar functions $E_{x,y,z}^{(n)}(z)$ and $H_{x,y,z}^{(n)}(z)$.

The RCWA was implemented using Mathematica™ after replacing $\mathbb{Z}$ by the set $\{0,\pm1,\pm2,\ldots,\pm N_t\}$ in the foregoing equations. A numerically stable algorithm[25–27] was used to find the reflection amplitudes $\{r_{s,p}^{(n)}\}_{n=-N_t}^{N_t}$ and transmission amplitudes $\{t_{s,p}^{(n)}\}_{n=-N_t}^{N_t}$ in terms of the incidence amplitudes $\{a_{s,p}^{(n)}\}_{n=-N_t}^{N_t}$. Thus,

- the total reflectance

$$R_p = \sum_{n=-N_t}^{n=N_t} \{|r_p^{(n)}|^2 \,\mathrm{Re}(k_z^{(n)}/k_z^{(0)})\} \tag{12}$$

for a p-polarized incident plane wave ($a_p^{(n)} = \delta_{n0}$ and $a_s^{(n)} \equiv 0\ \forall\ n \in \mathbb{Z}$) and

- the total reflectance

$$R_s = \sum_{n=-N_t}^{n=N_t} \{|r_s^{(n)}|^2 \,\mathrm{Re}(k_z^{(n)}/k_z^{(0)})\} \tag{13}$$

for an s-polarized incident plane wave ($a_s^{(n)} = \delta_{n0}$ and $a_p^{(n)} \equiv 0\ \forall\ n \in \mathbb{Z}$) were computed as functions of the angle of incidence θ and the free-space wavelength λ_0. The region $L_d < z < L_d + L_g$ was divided into 2-nm-thick slices and the value of N_t was sufficiently large to assure the convergence of the modal reflectances $\{|r_{s,p}^{(n)}|^2\}_{n=-N_t}^{N_t}$

2.2 *Planar Metallic Back-Reflector: Canonical Boundary-Value Problem*

To predict the wavenumbers $k_x^{(n)}$ of Floquet harmonics (of order n) that SPP waves would manifest as in the problem described in Sec. 2.1,[23] let us consider the underlying canonical boundary-value problem where one half-space (say, $z < 0$) is occupied by a metal with relative permittivity ϵ_m and the other half-space ($z > 0$) by a periodically nonhomogeneous dielectric material such that each period of it contains the three $p-i-n$ cells (but not the AZO layers) present in the region $0 < z < L_d$ in Fig. 1.

Let an SPP wave propagate parallel to the x-axis with wavenumber q and attenuate as $z \to \pm\infty$. Therefore, in the region $z < 0$, the electric and magnetic field phasors may be written as

$$\mathbf{E}(\mathbf{r}) = \left[b_p\left(\frac{\alpha_m}{k_0}\hat{\mathbf{u}}_x + \frac{q}{k_0}\hat{\mathbf{u}}_z\right) + b_s\hat{\mathbf{u}}_y\right]\exp[i(qx-\alpha_m z)], \quad z<0, \tag{14}$$

and

$$\mathbf{H}(\mathbf{r}) = \eta_0^{-1}\left[-b_p\epsilon_m\hat{\mathbf{u}}_y + b_s\left(\frac{\alpha_m}{k_0}\hat{\mathbf{u}}_x + \frac{q}{k_0}\hat{\mathbf{u}}_z\right)\right] \times \exp[i(qx-\alpha_m z)], \quad z<0, \tag{15}$$

where $q^2 + \alpha_m^2 = k_0^2\epsilon_m$, q is complex valued, and $\mathrm{Im}(\alpha_m) > 0$ for attenuation as $z \to -\infty$. Here, b_p and b_s are unknown coefficients with the same units as the electric field, with the subscripts p and s, respectively, denoting the s- and p-polarization states. The field phasors in the half-space $z > 0$ can be written as

$$\left.\begin{aligned}\mathbf{E}(\mathbf{r}) &= \mathbf{e}(z)\exp(iqx) \\ \mathbf{H}(\mathbf{r}) &= \mathbf{h}(z)\exp(iqx)\end{aligned}\right\}, \quad z>0, \tag{16}$$

where the functions $\mathbf{e}(z)$ and $\mathbf{h}(z)$ are not known.

After imposing the standard boundary conditions at the interface $z = 0$ plus the condition that the field phasors must decay as $z \to \pm\infty$, a dispersion equation was obtained and solved using the Newton–Raphson method[28] for the wavenumber q as a function of λ_0. The formulation has been explained in detail elsewhere.[16,29]

3 Numerical Results and Discussion

For the illustrative numerical results presented in this section, the various layers of the tandem solar cell in Fig. 1 were assumed to be made of a-Si alloys as follows:

- a-Si:H with bandgap $E_g = 1.8$ eV for all n-type layers and layers with thickness d_{1p} and d_{3i},
- a-$Si_{1-u}C_u$:H with bandgap $E_g = 1.95$ eV for the layers with thickness d_{2p} and d_{3p},
- a-$Si_{1-u}Ge_u$:H with bandgap $E_g = 1.39$ eV for the intrinsic layer of thickness d_{1i}, and
- a-$Si_{1-u}Ge_u$:H with bandgap $E_g = 1.58$ eV for the intrinsic layer of thickness d_{2i}.

Thus the tandem solar cell would function as a spectrum-splitting solar cell.[1,20] All the n- and p-type layers were taken to be 20-nm thick, and the thickness of all intrinsic layers was taken to be 200 nm. The relative permittivities of the a-Si alloys as functions of λ_0 are presented in Fig. 2. They were computed using a model provided by Ferlauto et al.[20] The thicknesses of the two AZO layers were set as $d_T = 100$ nm and $d_a = 140$ nm. The refractive index of AZO was obtained as a function of λ_0 by using a single-oscillator model developed for AZO films deposited by reactive magnetron sputtering at a substrate temperature of 170°C.[30] The imaginary part of the refractive index of AZO is negligible in the visible and the near-infrared regimes.[30] The information provided in this paragraph is sufficient to specify $\epsilon_d(z)$.

The metal was taken to be silver, and its relative permittivity was taken from a standard source.[31,32] Moreover, we set $L_m = 30$ nm.

3.1 *Planar Back-Reflector*

Before we present the results for the periodically corrugated metallic back-reflector, let us present the results when the back-reflector is planar (i.e., $L_g = 0$). The total reflectances R_p and R_s are presented in Fig. 3 for $\theta \in [0, 70]$ deg and $\lambda_0 \in [400,900]$ nm. The corresponding absorptances are

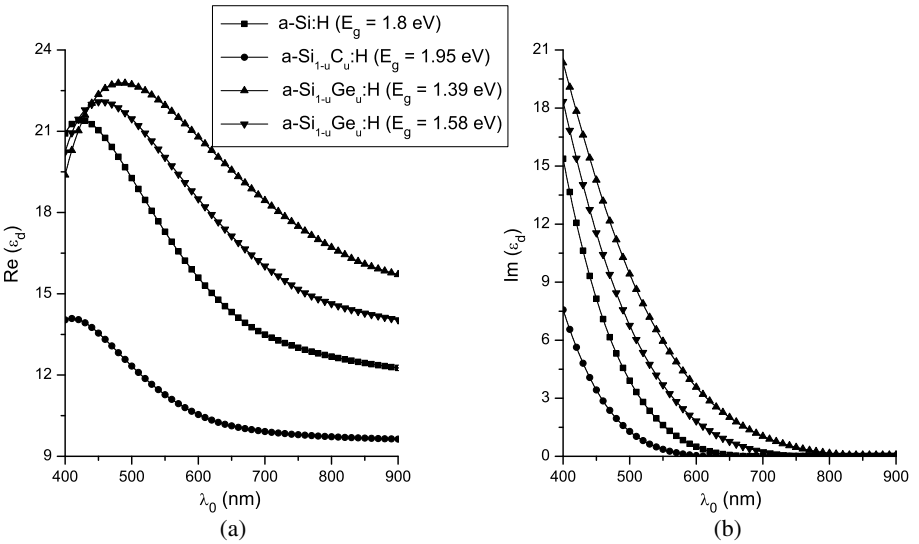

Fig. 2 (a) Real and (b) imaginary parts of the relative permittivities of a-Si alloys as functions of λ_0. These materials were used for the tandem solar cell, as detailed at the beginning of Sec. 3.

$A_p = 1 - R_p$ and $A_s = 1 - R_s$, because transmittances are negligible as the thickness L_m exceeds the penetration depth of silver. Since the absorption of light by AZO is negligible, light is absorbed only by the $p - i - n$ cells and the metal. Furthermore, the nonspecular components of the reflected field are absent because the metallic back-reflector is planar and $N_t = 0$ then suffices.

Figure 3 shows that both total reflectances are very low when $\lambda_0 < 700$ nm, but both are very high when $\lambda_0 > 750$ nm. This dimorphism is due to the higher values of the imaginary parts of the relative permittivities of the a-Si alloys at shorter wavelengths. Therefore, considerable room for enhancement of the absorption of light by the semiconductor layers is available when $\lambda_0 > 700$ nm.

The absence of sharply defined bands with low reflectance in Fig. 3 indicates that no SPP waves are excited. Parenthetically, we note that high-phase-speed SPP waves can indeed be excited with a planar interface if the partnering dielectric material is several-periods thick[33]; but, as these SPP waves will not play a significant role in enhancing the absorption of light in solar cells, their excitation was not investigated.

3.2 *Simple Surface-Relief Grating as the Back-Reflector*

Let us next consider that the tandem solar cell is backed by a simple surface-relief grating with

$$g(x) = L_d + L_g\left[1 - \sin\left(\frac{2\pi x}{L_x}\right)\right] \tag{17}$$

as the grating-shape function.

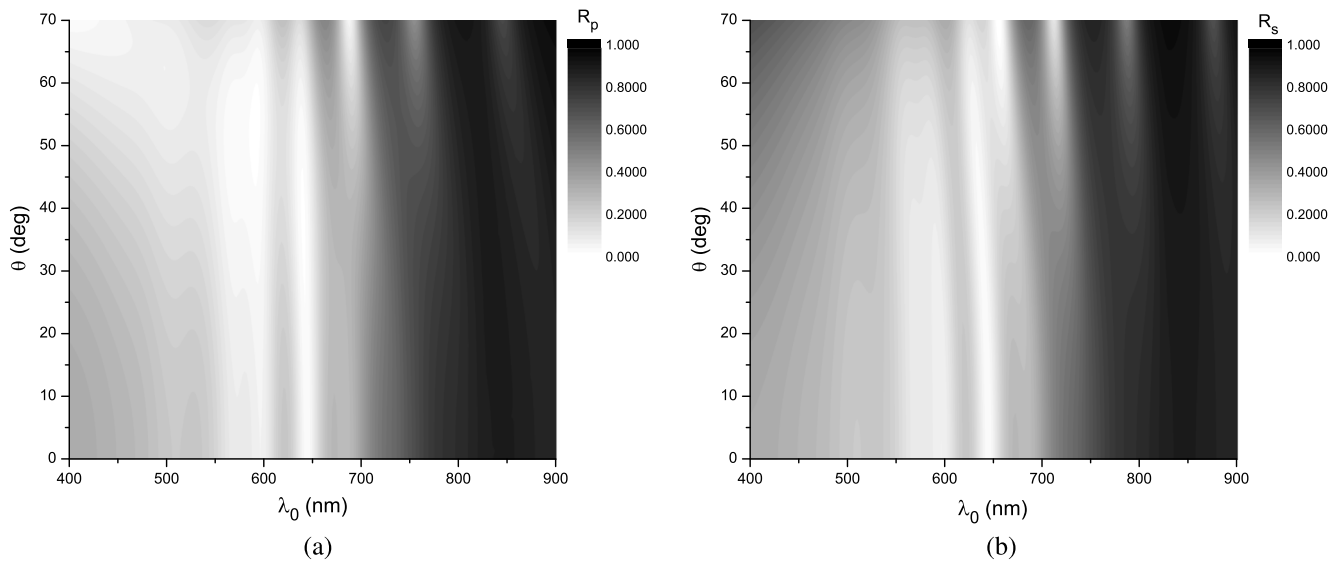

Fig. 3 Total reflectances (a) R_p and (b) R_s as functions of θ and λ_0 when $L_g = 0$. No nonspecular Floquet harmonics and no SPP waves are excited due to the absence of the periodic corrugations in the metallic back-reflector.

For the computation of the reflectances, the wavelength range was restricted to $\lambda_0 \in [450,900]$ nm because of convergence problems with the RCWA when $\lambda_0 \in [400,450]$ nm. This is due to the fact that a-Si alloys are highly dissipative for $\lambda_0 \in [400,450]$ nm, as can be seen from the plots of the real and the imaginary parts of the relative permittivities in Fig. 2. However, the high dissipation in turn implies that the light absorption efficiency in this narrow spectral regime is very high and does not offer much room for improvement.

3.2.1 L_x = 400 nm

Suppose next that the period $L_x = 400$ nm and the trough-to-crest height $L_g = 80$ nm. We set $N_t = 9$ after ascertaining that the RCWA provided converged solutions. The total reflectances R_p and R_s as functions of θ and λ_0 are presented in Figs. 4(a) and 4(b), respectively. Also in the same figure, the angle

$$\theta_{\mathrm{SPP}} = \sin^{-1}\left[\frac{\mathrm{Re}(q)}{k_0} - n\frac{\lambda_0}{L_x}\right] \tag{18}$$

is plotted in relation to λ_0 when an SPP wave is predicted to be excited as a Floquet harmonic of order n,[23] q being the wavenumber of either a p- or an s-polarized SPP wave delivered by the solution of the canonical boundary-value problem described in Sec. 2.2. As the transmittances were found to be negligible, the higher that the total reflectance is, the lower is the corresponding absorptance.

The two upper panels in Fig. 4 show the presence of low-reflectance bands when $\lambda_0 > 750$ nm. These bands could be due to the excitation of either SPP waves or waveguide modes[34] that propagate in the bulk of the tandem solar cell. The two lower panels in Fig. 4 show the locations in $\lambda_0 \times \theta$ space where SPP waves are predicted to be excited for the chosen solar cell. Comparisons of Figs. 4(a) and 4(c), and of Figs. 4(b) and 4(d), suffice to identify the low-reflectance bands that represent the excitation of SPP waves. Clearly then, multiple p- and s-polarized SPP waves are

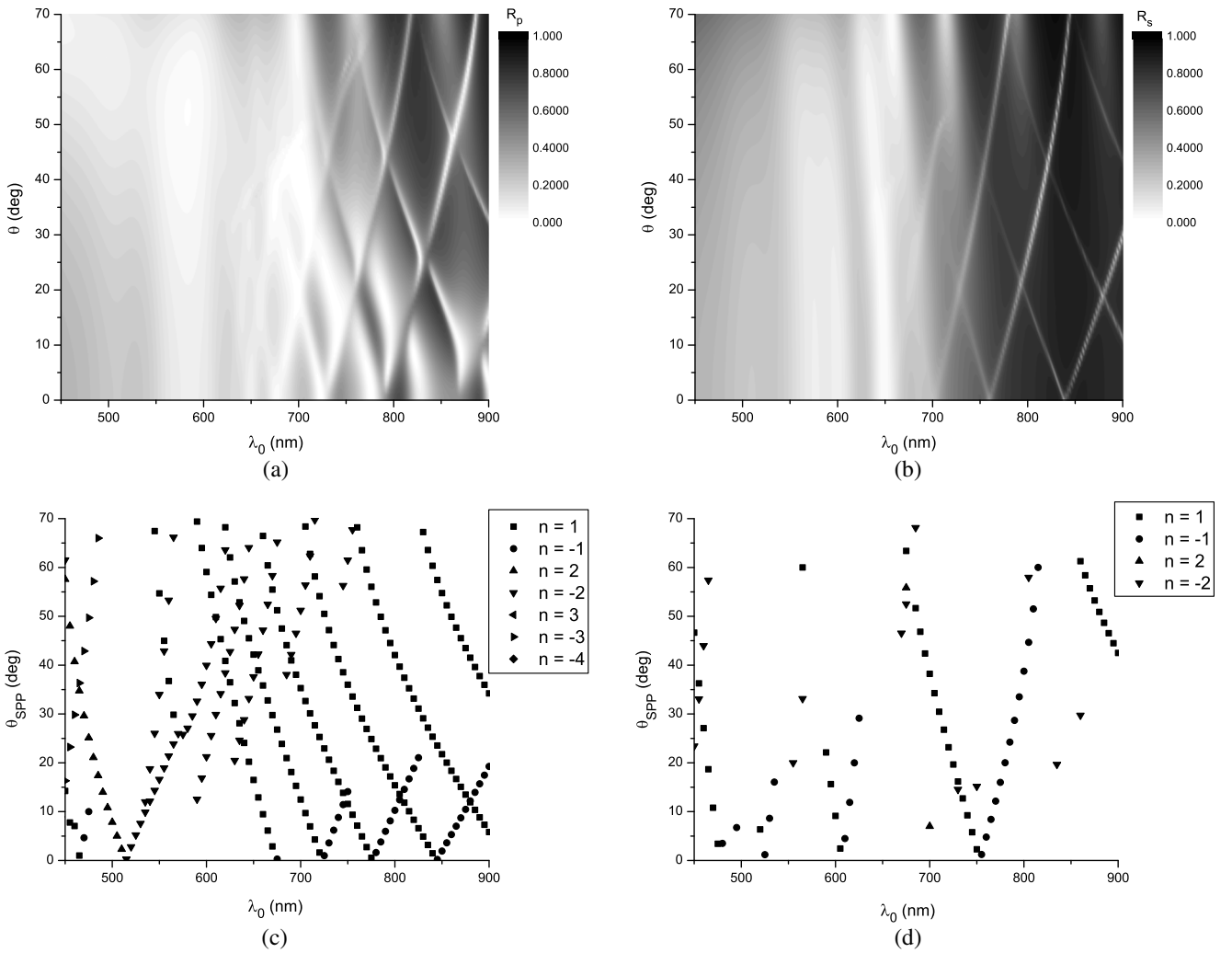

Fig. 4 Total reflectances (a) R_p and (b) R_s as functions of θ and λ_0 when the metallic back-reflector is sinusoidally corrugated with period L_x = 400 nm and depth L_g = 80 nm, per Eq. (17). Values of θ_{SPP} defined in Eq. (18) in relation to λ_0 when wavenumber $k_x^{(n)}$ of a Floquet harmonic of order n is the same as wavenumber q of (c) p- and (d) s-polarized SPP waves delivered by the solution of the underlying canonical boundary-value problem.

excited due to the periodic corrugation of the metallic back-reflector. The low-reflectance bands that do not correspond to the branches in Figs. 4(c) and 4(d) most likely represent the excitation of waveguide modes that are guided by the tandem solar cell.

Comparisons of Figs. 3(a) and 4(a), and of Figs. 3(b) and 4(b), show that R_p and R_s are generally smaller for $\lambda_0 > 700$ nm, when the metallic back-reflector is periodically corrugated than when it is planar. The decreases in R_p and R_s are surely due to the excitation of SPP waves and waveguide modes, thereby resulting in enhanced absorption of light by the tandem solar cell. The decrease in R_p is more than the decrease in R_s, which is in line with the theoretical prediction from the canonical boundary-value problem of a smaller number of s-polarized SPP waves than of p-polarized SPP waves.

The absence of the low-reflectance bands (representing the excitation of SPP waves) for both linear polarization states when $\lambda_0 < 700$ nm, even though the canonical boundary-value problem predicts the excitation of SPP waves, is inconsequential. This is because the absorption of light by the tandem solar cell is very high in this spectral regime. Most likely, those bands are not easily evident.

3.2.2 L_x = 500 nm

Let us now increase the period of corrugations to $L_x = 500$ nm, but $L_g = 80$ nm remains fixed. The RCWA algorithm delivered converged reflectances for $N_t = 13$.

The total reflectances R_p and R_s are presented as functions of θ and λ_0 in Figs. 5(a) and 5(b), respectively. The points in $\lambda_0 \times \theta$ space when either a p- or an s-polarized SPP wave is predicted to be excited are identified in Figs. 5(c) and 5(d), respectively. Comparisons of Figs. 4(c) and 5(c), and of Figs. 4(d) and 5(d), show that the points in $\lambda_0 \times \theta$ space when $L_x = 500$ nm are at different positions and are different in number for $L_x = 500$ nm than for $L_x = 400$ nm for both the linear polarization states. Parenthetically, we note that the wavenumbers q of SPP waves (for any given λ_0) obtained by the solution of the underlying canonical boundary-value problem are independent of the period L_x of the corrugations; however, the condition $k_0 \sin\theta_{\rm SPP} + n\frac{2\pi}{L_x} \approx {\rm Re}(q)$ that needs to be satisfied for those SPP waves to be excited involves the period L_x.

Comparisons of Figs. 5(a) and 5(c), and of Figs. 5(b) and 5(d), allow us to conlcude that several low-reflectance bands (for $\lambda_0 > 700$ nm) are due to the excitation of SPP waves.

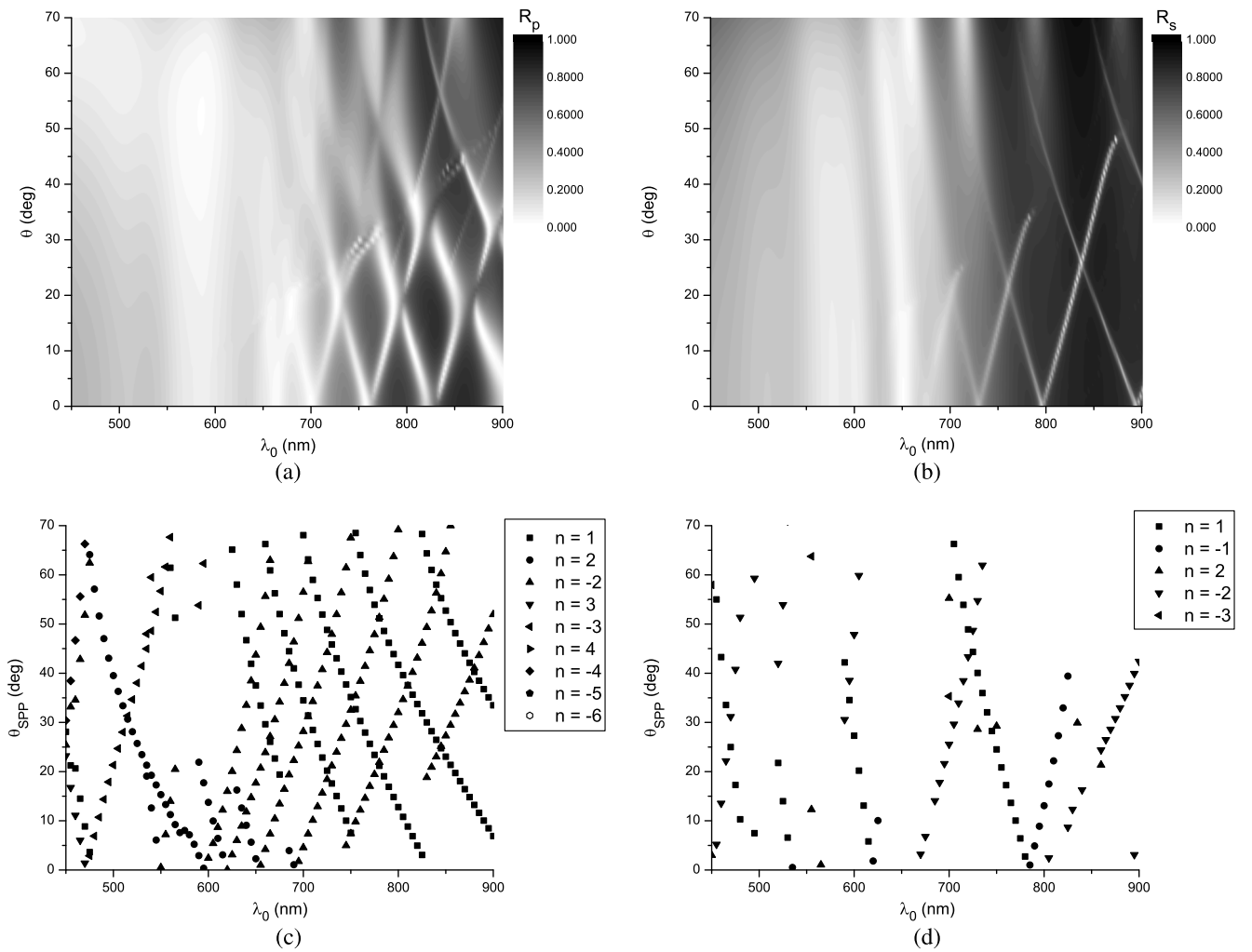

Fig. 5 Same as Fig. 4 except that $L_x = 500$ nm.

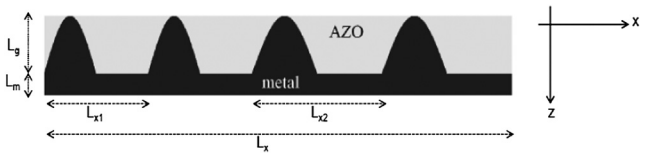

Fig. 6 Schematic of the compound surface-relief grating when $g(x)$, $x \in (0, L_x)$ is given by Eq. (19) with $N_1 = N_2 = 2$.

This excitation of multiple SPP waves is accompanied by overall low reflectances in the near-infrared spectral regime ($\lambda_0 > 700$ nm) as compared to Fig. 3 for the planar metallic back-reflector.

3.3 *Compound Surface-Relief Grating as the Back-Reflector*

An SPP wave is excited in the grating-coupled configuration when the condition $k_0 \sin\theta_{\rm SPP} + n\frac{2\pi}{L_x} \approx {\rm Re}(q)$ is met.[16,23] To increase the number of SPP waves, a compound surface-relief grating with each period having several periods of more than one simple surface-relief grating can be used.[35,36] For this purpose, we chose a compound grating with

$$g(x) = \begin{cases} L_d + L_g\left[1 - \sin\left(2\pi\frac{x}{L_{x1}}\right)\right], & x \in (0, N_1 L_{x1}) \\ L_d + L_g\left[1 - \sin\left(2\pi\frac{x-N_1L_{x1}}{L_{x2}}\right)\right], & x \in (N_1L_{x1}, N_1L_{x1} + N_2L_{x2} = L_x) \end{cases}, \tag{19}$$

specified in the reference unit cell of the region $L_d < z < L_d + L_g$. A schematic representation of the compound grating is shown in Fig. 6. The density plots of the reflectances R_p and R_s as functions of θ and λ_0 for a compound grating with $N_1 = N_2 = 2$, $L_{x1} = 401$ nm, $L_{x2} = 501$ nm, and $L_g = 80$ nm are given in Fig. 7. We chose each period of the compound grating to comprise two periods each of the simple sinusoidal gratings with periods $L_{x1} = 401$ nm and $L_{x2} = 501$ nm—instead of $L_{x1} = 400$ nm and $L_{x2} = 500$ nm—to avoid difficulties in computing the Fourier coefficients used in Eq. (10). Moreover, $N_t = 16$ was chosen after ensuring the convergence of the reflectances.

The low-reflectance bands in Fig. 7 representing the excitation of SPP waves could either be attributed to an individual simple surface-relief grating in the compound grating or the compound grating itself, though the efficiency of the excitation is generally smaller with the compound grating than with either of the simple grating alone.[36] Furthermore, not all SPP waves excited by individual simple gratings may be excited by the compound grating. A comparison of Fig. 7 with Fig. 3 shows that the reflectance in the near-infrared regime is generally lower when a compound grating is used than when the metallic back-reflector is planar.

3.4 *Solar-Spectrum-Integrated Absorption Efficiency*

The solar-spectrum-integrated (SSI) absorption efficiency is defined by[37]

$$\eta(\theta) = \frac{1}{\int_{\lambda_{\rm min}}^{\lambda_{\rm max}} \lambda_0 S(\lambda_0)\,{\rm d}\lambda_0} \times \int_{\lambda_{\rm min}}^{\lambda_{\rm max}} \frac{2 - R_p(\lambda_0,\theta) - R_s(\lambda_0,\theta)}{2}\,\lambda_0 S(\lambda_0)\,{\rm d}\lambda_0, \tag{20}$$

for unpolarized light coming from the sun, where $S(\lambda_0)$ is the solar irradiance spectrum for AM1.5.[38] The SSI absorption efficiency is plotted in Fig. 8 as a function of θ when the metallic back-reflector is (1) planar, (2) the simple grating of Sec. 3.2.1, (3) the simple grating of Sec. 3.2.2, or (4) a

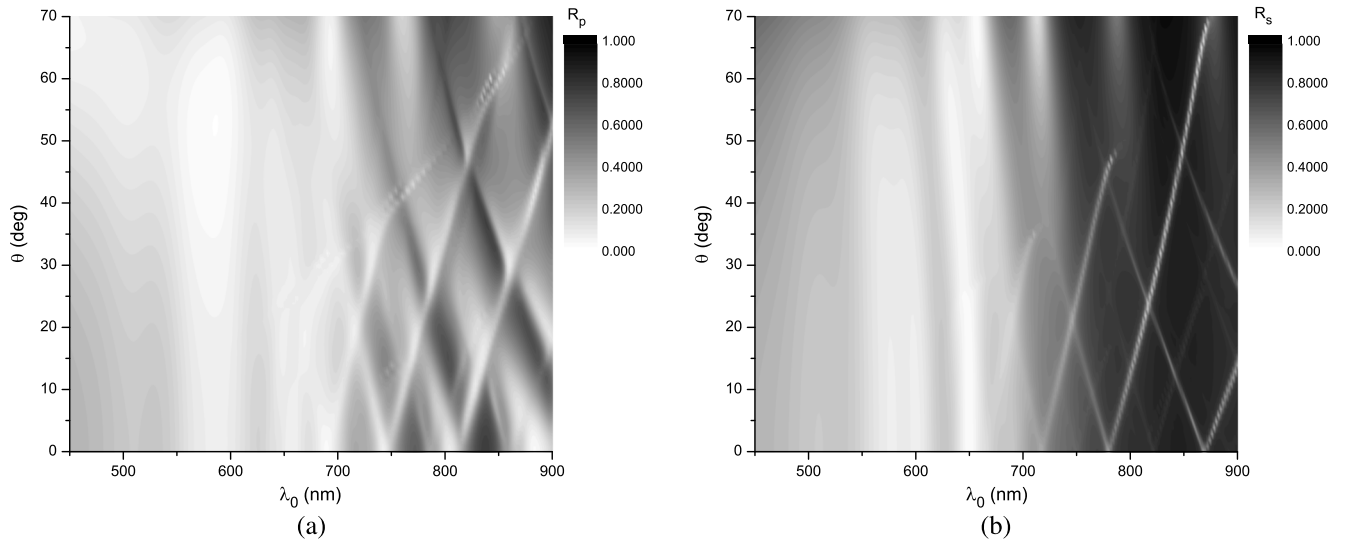

Fig. 7 Total reflectances (a) R_p and (b) R_s as functions of θ and λ_0 when the solar cell is backed by a compound grating defined by Eq. (19) with $L_{x1} = 401$ nm, $L_{x2} = 501$ nm, and $L_g = 80$ nm.

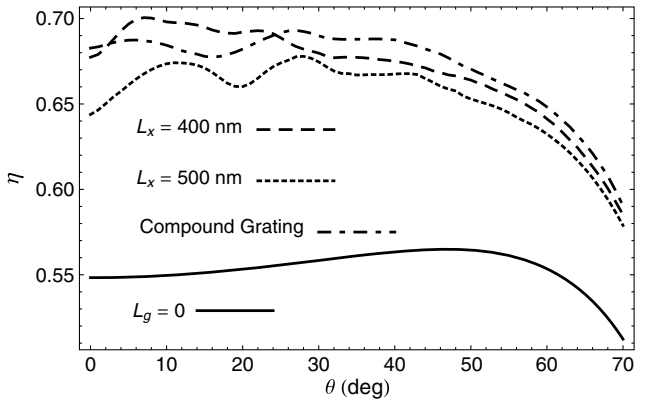

Fig. 8 SSI absorption efficiency η as a function of the incidence angle θ when $\lambda_{min} = 450$ nm and $\lambda_{max} = 900$ nm. The dashed and dotted lines represent simple gratings ($L_g = 80$ nm), the chain-dashed line represents the compound grating defined by Eq. (19) with $L_{x1} = 401$ nm and $L_{x2} = 501$ nm ($L_g = 80$ nm), and the solid line represents the planar back-reflector.

compound grating of Sec. 3.3, with $\lambda_{min} = 450$ nm and $\lambda_{max} = 900$ nm. The figure shows that η increased by up to 20% when the solar cell is backed by a periodically corrugated reflector than a planar reflector. For $\theta \in (2, 23)$ deg, the simple grating with period $L_x = 400$ nm gives the highest SSI absorption efficiency. When either $\theta \approx 0$ deg or $\theta \in (23, 70)$ deg, the compound grating yields the highest SSI absorption efficiency.

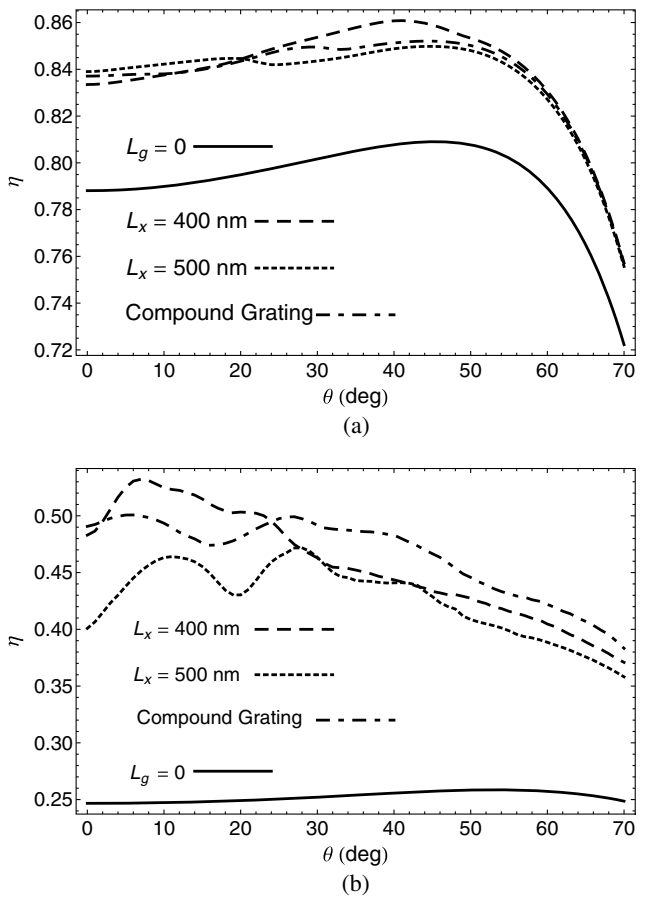

Fig. 9 Same as Fig. 8 except that (a) $\lambda_{min} = 450$ nm and $\lambda_{max} = 700$ nm, and (b) $\lambda_{min} = 700$ nm and $\lambda_{max} = 900$ nm.

To delineate the enhancement of absorption efficiency in the near-infrared spectral regime, the SSI absorption efficiencies are presented in Figs. 9(a) and 9(b) when $\lambda_{min} = 450$ nm and $\lambda_{max} = 700$ nm, and $\lambda_{min} = 700$ nm and $\lambda_{max} = 900$ nm, respectively. Figure 9(a) shows that η is enhanced up to 5% only when $\lambda_0 \in [450, 700]$ nm. This is due to the fact that semiconductor materials used in the solar cell are highly dissipative in this spectral regime. Furthermore, in this spectral regime, both the simple gratings and the compound grating have very similar effects on η. This is also evident from Fig. 9(a) since η is about 80% over a wide range of the incidence angle θ even when the metallic back-reflector is planar.

The plots of η in Fig. 9(b), however, show an enhancement of up to 100% when $\lambda_0 \in [700, 900]$ nm. Let us repeat that multiple SPP waves excited with either the simple or the compound grating are all dominant in this spectral regime. Therefore, the enhancement in η can be attributed to the excitation of multiple SPP waves.

4 Concluding Remarks

The effect of multiple SPP waves on the SSI absorption efficiency of a thin-film tandem solar cell made of a-Si alloys with a periodically corrugated metallic back-reflector was theoretically investigated. The boundary-value problem to find the total reflectances as functions of the free-space wavelength $\lambda_0 \in [450, 900]$ nm and the angle of incidence $\theta \in [0, 70]$ deg for incident linearly polarized plane waves was set up and solved for a typical tandem solar cell. The low-reflectance bands representing the excitation of SPP waves by simple gratings were identified by comparing the total-reflectance spectrums with the solution of the underlying canonical boundary-value problem. A compound grating with each period occupying several periods of two simple gratings was also investigated.

The total reflectance in the near-infrared regime was found to decrease for both linear polarization states when the metallic back-reflector is periodically corrugated than when it was planar. The identification of multiple SPP waves showed that most of the decrease in total reflectance results from the excitation of SPP waves. Furthermore, the use of different periods for the corrugations of the metallic back-reflector showed that the position of low-reflectance bands in the $\lambda_0 \times \theta$ space can be changed by changing the period of the corrugations. A compound grating was found to deliver a larger number of SPP waves than a simple grating, but the excitation efficiency was generally lower than when a simple grating was used.

The SSI absorption efficiency as a function of the incidence angle using an AM1.5 solar spectrum showed that an enhancement of the absorption efficiency of as much as 20% is achievable when the back reflector is periodically corrugated. A further analysis of the efficiency by dividing the spectral regime into $\lambda_0 \in [450, 700]$ nm and $\lambda_0 \in [700, 900]$ nm showed that most of the enhancement in absorption comes from the enhancement in the near-infrared spectral regime.

Let us note that the absorption efficiency of the tandem solar cell depends not only on the period L_x of the corrugations of the metallic back-reflector, but also on the other parameters such as the depth, shape, and the duty cycle of the corrugations.[37] Furthermore, the choice of periodically

corrugated back-reflector depends on the thicknesses and the materials used for making a solar cell. Since multiple SPP waves are guided due to the periodic nonhomogeneity of the partnering semiconductor material, an enhancement in the absorption efficiency should be expected in any thin-film solar cell. Therefore, we hope that our numerical studies have provided experimentalists with some useful guidelines to exploit surface multiplasmonics[16] for harvesting solar energy not only in those cells that are made of a-Si alloys but also of compound semiconductor materials.

Acknowledgments

This work was partially supported by US National Science Foundation grant DMR-1125591. The authors thank Liu Liu, A. Shoji Hall, Greg D. Barber, Theresa S. Mayer, and Thomas E. Mallouk of the Pennsylvania State University for helpful discussions during the course of this work. A. L. thanks the Charles G. Binder Endowment at Penn State for ongoing support of his research.

References

1. S. J. Fonash, *Solar Cell Device Physics*, 2nd Ed., Academic Press, Burlington, MA (2010).
2. S. K. Dhungel et al., "Double-layer antireflection coating of MgF_2/SiN_x for crystalline silicon solar cells," *J. Korean Phys. Soc.* **49**(3), 885–889 (2006).
3. S. A. Boden and D. M. Bagnall, "Sunrise to sunset optimization of thin film antireflective coatings for encapsulated, planar silicon solar cells," *Prog. Photovolt: Res. Appl.* **17**, 241–252 (2009).
4. J.-Y. Chu et al., "17.2% efficiency multicrystalline solar cells by optimizing structure of the MgF_2/SiN_x double antireflection layer," *J. Photon. Energy* **1**(1), 017001 (2011).
5. R. M. Swanson and R. A. Sinton, "High-efficiency silicon solar cells," in *Advances in Solar Energy*, K. W. Bauer, Ed., Vol. 6, pp. 427–484, Plenum Press, New York (1990).
6. P. Verlinden et al., "The surface texturization of solar cells: a new method with V-grooves with controllable sidewall angles," *Sol. Energy Mater. Sol. Cells* **26**(1), 71–78 (1992).
7. N. Yamada et al., "Characterization of antireflection moth-eye film on crystalline silicon photovoltaic module," *Opt. Express* **19**(S2), A118–A125 (2011).
8. G. Aijuan et al., "Effect of the back surface topography on the efficiency in silicon solar cells," *J. Semicond.* **30**(7), 074003 (2009).
9. P. Sheng, A. N. Bloch, and R. S. Stepleman, "Wavelength-selective absorption enhancement in thin-film solar cells," *Appl. Phys. Lett.* **43** (6), 579–581 (1983).
10. C. Heine and R. H. Morf, "Submicrometer gratings for solar energy applications," *Appl. Opt.* **34**(14), 2476–2482 (1995).
11. M. A. Green and S. Pillai, "Harnessing plasmonics for solar cells," *Nat. Photon.* **6**(3), 130–132 (2012).
12. L. M. Anderson, "Parallel-processing with surface plasmons: a new strategy for converting the broad solar spectrum," *Proc. 16th IEEE Photovoltaic Specialist Conf.*, San Diego, CA, Vol. 1, pp. 371–377 (1982).
13. L. M. Anderson, "Harnessing surface plasmons for solar energy conversion," *Proc. SPIE* **408**, 172–178 (1983).
14. H. A. Atwater and A. Polman, "Plasmonics for improved photovoltaic devices," *Nat. Mater.* **9**(3), 205–213 (2010).
15. S. A. Maier, *Plasmonics: Fundamentals and Applications*, Springer, New York (2007).
16. J. A. Polo, Jr., T. G. Mackay, and A. Lakhtakia, *Electromagnetic Surface Waves: A Modern Perspective*, Elsevier, Waltham (2013).
17. V. E. Ferry et al., "Plasmonic nanostructure design for efficient light coupling into solar cells," *Nano Lett.* **8**(12), 4391–4397 (2008).
18. M. Faryad and A. Lakhtakia, "Enhanced absorption of light due to multiple surface-plasmon-polariton waves," *Proc. SPIE* **8110**, 81100F (2011).
19. B. B. Van Aken et al., "PECVD deposition of a-Si:H and μc-Si:H using a linear RF source," *Proc. SPIE* **6651**, 66510C (2007).
20. A. S. Ferlauto et al., "Analytical model for the optical functions of amorphous semiconductors from the near-infrared to ultraviolet: applications in thin film photovoltaics," *J. Appl. Phys.* **92**(5), 2424–2436 (2002).
21. M. G. Moharam and T. K. Gaylord, "Diffraction analysis of dielectric surface-relief gratings," *J. Opt. Soc. Am.* **72**(10), 1385–1392 (1982).
22. L. Li, "Multilayer modal method for diffraction gratings of arbitrary profile, depth, and permittivity," *J. Opt. Soc. Am. A* **10**(12), 2581–2591 (1993).
23. M. Faryad and A. Lakhtakia, "Grating-coupled excitation of multiple surface plasmon-polariton waves," *Phys. Rev. A* **83**(1), 013814 (2011).
24. M. Faryad et al., "Excitation of multiple surface-plasmon-polariton waves guided by a periodically corrugated interface of a metal and a periodic multilayered isotropic dielectric material," *J. Opt. Soc. Am. B* **29**(4), 704–713 (2012).
25. M. G. Moharam, E. B. Grann, and D. A. Pommet, "Formulation for stable and efficient implementation of the rigorous coupled-wave analysis of binary gratings," *J. Opt. Soc. Am. A* **12**(5), 1068–1076 (1995).
26. F. Wang, M. W. Horn, and A. Lakhtakia, "Rigorous electromagnetic modeling of near-field phase-shifting contact lithography," *Microelectron. Eng.* **71**(1), 34–53 (2004).
27. N. Chateau and J.-P. Hugonin, "Algorithm for the rigorous coupled-wave analysis of grating diffraction," *J. Opt. Soc. Am. A* **11**(4), 1321–1331 (1994).
28. Y. Jaluria, *Computer Methods for Engineering*, Taylor & Francis, Washington (1996).
29. M. Faryad and A. Lakhtakia, "On surface plasmon-polariton waves guided by the interface of a metal and a rugate filter with sinusoidal refractive-index profile," *J. Opt. Soc. Am. B* **27**(11), 2218–2223 (2010).
30. X.-Y. Gao, Y. Liang, and Q.-G. Lin, "Analysis of the optical constants of aluminum-doped zinc oxide films by using the single-oscillator model," *J. Korean Phys. Soc.* **57**(4), 710–714 (2010).
31. E. D. Palik, Ed., *Handbook of Optical Constants of Solids*, Academic Press, Boston (1985).
32. http://refractiveindex.info/?group=METALS&material=Silver (8 May 2013).
33. M. R. M. Atalla, M. Faryad, and A. Lakhtakia, "On surface plasmon-polariton waves guided by the interface of a metal and a rugate filter with a sinusoidal refractive-index profile. Part II: High-phase-speed solutions," *J. Opt. Soc. Am. B* **29**(11), 3078–3086 (2012).
34. N. S. Kapany and J. J. Burke, *Optical Waveguides*, Academic Press, New York (1972).
35. I. Dolev et al., "Multiple coupling of surface plasmons in quasiperiodic gratings," *Opt. Lett.* **36**(9), 1584–1586 (2011).
36. M. Faryad and A. Lakhtakia, "Excitation of multiple surface-plasmon-polariton waves using a compound surface-relief grating," *J. Nanophoton.* **6**(1), 061701 (2012).
37. M. Solano et al., "Optimization of the absorption efficiency of an amorphous-silicon thin-film tandem solar cell backed by a metallic surface-relief grating," *Appl. Opt.* **52**(5), 966–979 (2013).
38. http://pveducation.org/pvcdrom/appendices/standard-solar-spectra (23 July 2013).

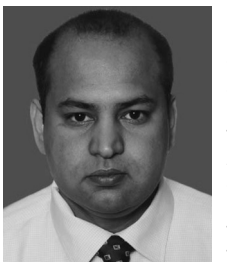

Muhammad Faryad received MSc and MPhil degrees in electronics from the Quaid-i-Azam University, Pakistan, in 2006 and 2008, respectively, and the PhD degree in engineering science and mechanics from the Pennsylvania State University, USA, in 2012. Currently, he is a postdoctoral scholar at the Pennsylvania State University. His research interests include sculptured thin films, solar cells, and electromagnetic surface waves. He is a member of Optical Society of America and SPIE.

Akhlesh Lakhtakia received degrees from the Banaras Hindu University (BTech and DSc) and the University of Utah (MS and PhD), in electronics engineering and electrical engineering, respectively. He is the Charles Godfrey Binder (Endowed) Professor of Engineering Science and Mechanics at the Pennsylvania State University, and presently serves as the Editor-in-Chief of the *Journal of Nanophotonics*. His current research interests include nanotechnology, bioreplication, forensic science, surface multiplasmonics, and complex materials including metamaterials and sculptured thin films. He is a fellow of SPIE, Optical Society of America, American Association for the Advancement of Science, American Physical Society, and Institute of Physics (UK). He was the sole recipient of the 2010 SPIE Technical Achievement Award.